THE JOURNAL OF PHYSICAL CHEMISTRY C
A JOURNAL OF THE AMERICAN CHEMICAL SOCIETY

pubs.acs.org/JPCC

Article

Frequency and Amplitude Optimizations for Magnetic Particle Spectroscopy Applications

Vinit Kumar Chugh, Arturo di Girolamo, Venkatramana D. Krishna, Kai Wu,* Maxim C-J Cheeran,* and Jian-Ping Wang*

Cite This: J. Phys. Chem. C 2023, 127, 450−460

Read Online

ACCESS | Metrics & More | Article Recommendations | Supporting Information

ABSTRACT: Nowadays, there is a growing interest in the field of magnetic particle spectroscopy (MPS)-based bioassays. MPS monitors the dynamic magnetic response of surface-functionalized magnetic nanoparticles (MNPs) upon excitation by an alternating magnetic field (AMF) to detect various target analytes. This technology has flourished in the past decade due to its low cost, low background magnetic noise interference from the biomatrix, and fast response time. A large number of MPS variants have been reported by different groups around the world, with applications ranging from disease diagnosis to foodborne pathogen detection and virus detection. However, there is an urgent need for guidance on how to optimize the sensitivity of MPS detection by choosing different types of MNPs, AMF modalities, and MPS assay strategies (i.e., volume- and surface-based assays). In this work, we systematically study the effect of AMF frequencies and amplitudes on the responses of single- and multicore MNPs under two extreme conditions, namely, the bound and unbound states. Our results show that some modalities such as dual-frequency MPS utilizing multicore MNPs are more suitable for surface-based bioassay applications, whereas single-frequency MPS systems using single- or multicore MNPs are better suited for volumetric bioassay applications. Furthermore, the bioassay sensitivities for these modalities can be further improved by a careful selection of AMF frequencies and amplitudes.

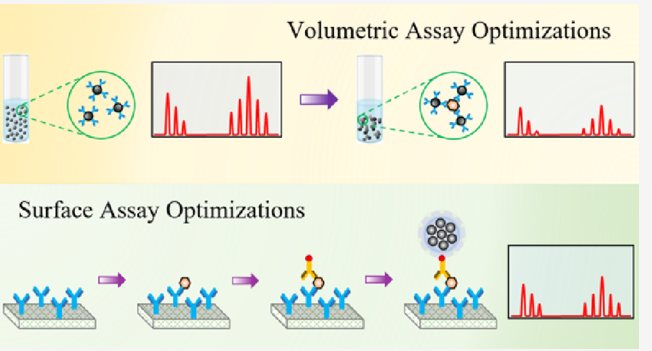

1. INTRODUCTION

Magnetic particle spectroscopy (MPS) is a technology derived from the noninvasive tomographic technique, magnetic particle imaging.[1,2] The idea of MPS was first conceived by Krause et al. and Nikitin et al. in 2006, respectively.[3,4] MPS detects the dynamic magnetic responses of magnetic nanoparticles (MNPs) upon the application of alternating magnetic fields (AMFs), namely, the driving fields. Over the last decade, MPS has been reported as a powerful tool for detecting blood viscosity and blood clot,[5,6] foodborne pathogens and toxins,[7−10] animal (e.g., Hepatitis B, H1N1, SARS-CoV-2, etc.)[11−17] and plant viruses (e.g., grapevine fanleaf virus, potato virus X, etc.),[18] hormones, cytokines, and other signaling molecules from body fluids.[19,20] Nowadays, there have emerged a variety of MPS platforms such as the single- and dual-frequency AMF implementations (categorized by the number of AMFs), the single- and multicore MNP-based assays (categorized by the structure of MNPs), and the volume- and surface-based assay strategies (categorized by the major contributing relaxation mechanisms).[12,14,21−24]

The MPS volumetric systems mainly rely on detecting subtle changes in the binding state of the MNP (binding to target analytes or cross-linked by the presence of target analytes), which results in a difference in the Brownian relaxation time and changes the magnetic response. Both single- and multicore MNPs combined with either single- or dual-frequency AMFs have been reported in the MPS volumetric systems. For example, 80 nm multicore MNPs and 30 nm single-core MNPs have been independently reported in the MPS volumetric system for the detection of SARS-CoV-2 proteins.[12,14] Multicore MNPs combined with single-frequency excitation field-driven MPS volumetric systems have also been widely reported for detecting a variety of disease biomarkers, such as thrombin and inflammation, and infection biomarkers.[20,23,25] It is worth mentioning that the MPS volumetric system shares some similarities with the magnetoreduction assay (MRA).[26−28] While both techniques detect the subtle changes of dynamic magnetic properties of MNPs from liquid phase, MRA uses a superconducting quantum interference device to

Received: October 26, 2022
Revised: December 14, 2022
Published: December 28, 2022

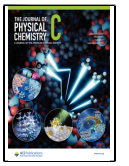

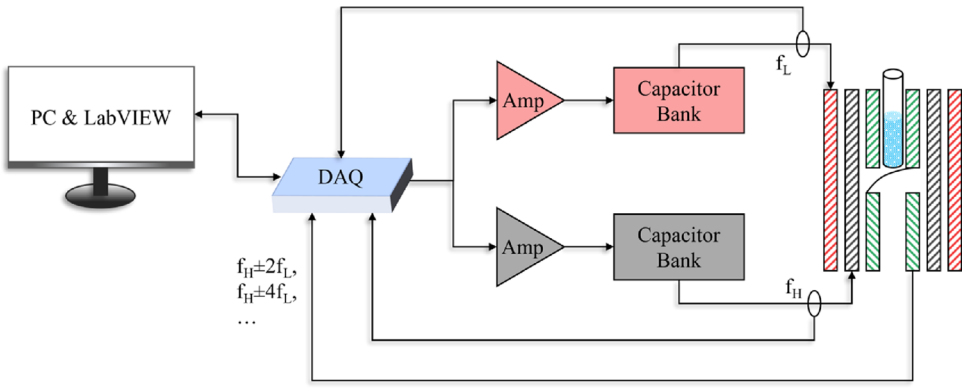

Figure 1. Schematic depiction of the modified benchtop MPS system with a resonating capacitor bank for low- and high-frequency driving coils.

detect the AC magnetic susceptibility χ_{AC} of MNPs, and MPS uses a pair of differentially wound Faraday coils (pick-up coils) to probe the dynamic magnetic moments of MNPs.

On the other hand, in MPS surface-based assay systems, the multicore MNPs driven by dual-frequency AMFs are widely reported for bioassay applications.[8,18,29−32] In this scenario, MNPs are captured on a solid substrate such as a nonmagnetic porous filter or a nitrocellulose membrane through the specific antibody−antigen−antibody sandwich assay structure. The dynamic magnetic responses are due to Néel relaxation of magnetic moments in these captured MNPs.

However, there is a lack of systematic studies on how to choose the right type of MNPs (single- or multicore structures) for certain MPS-based bioassay applications. Furthermore, guidelines for selecting optimal AMF frequencies and amplitudes for certain types of MNPs to achieve maximum bioassay sensitivity are urgently needed. In this work, we show an example of comparing the dynamic magnetic responses of two types of MNPs (i.e., 30 nm single-core SHS30 MNPs and 50 nm multicore SuperMag50 MNPs) under single- and dual-frequency AMFs. Two extreme bioassay conditions are designed, namely, the unbound MNPs suspended in liquid and the fully cross-linked MNP clusters in liquid. For the latter case, an excess number of biotinylated antibodies are added to ensure that all MNPs are bound, and Brownian relaxation is fully blocked. This condition also favors the study of a surface-based MPS assay since under this condition, only Néel relaxation governs the relaxation dynamics of MNP magnetization. Thus, the work reported herein tunes the three variables: MNP structures, AMF, and the MPS assay strategy intending to provide peers with insights on designing optimal settings for MPS-based bioassays.

The results show that the single-frequency MPS modality utilizing both the single- and multicore MNPs is suitable for volumetric bioassay applications. The sensitivity of this methodology can be further improved by utilizing higher excitation frequencies and amplitudes as both promote the Brownian relaxation mechanism of nanoparticles. It was also observed that in dual-frequency MPS systems, utilizing multicore MNPs and operating at higher excitation frequencies are optimal for surface-based bioassay applications, as Néel relaxation is the dominant relaxation mechanism. It was also noted that the sensitivity of such surface-based bioassay systems could be further optimized by a careful selection of high- and low-frequency excitation field amplitudes.

2. MATERIALS AND METHODS

2.1. Materials. The SHS30 MNPs are streptavidin-coated 30 nm single-core iron oxide nanoparticles, and SuperMag50 is 50 nm multicore iron oxide nanoparticles conjugated with streptavidin; both at concentrations of 1 mg/mL were obtained from Ocean NanoTech, USA. Biotinylated antibody goat anti-mouse IFN-γ with an antibody concentration of 0.4 μg/mL (2.67 nM) was obtained from R&D systems, USA (ELISA kit product number DY485-05, part number 840123). Phosphate-buffered saline (PBS) was purchased from Genesee Scientific, USA.

2.2. Static Magnetic Property Characterization. Static magnetic property characterization of the MNP samples was performed using the PPMS DynaCool system from Quantum Design. MNP samples were prepared by air-drying 10 μL of 1 mg/mL MNP solutions on a filter paper. Measurements were performed at 300 K and by varying the quasi-static field in the ±5000 Oe or ± 500 Oe ranges. Further information regarding the measured static properties is provided in the Supporting Information (Section S1).

2.3. Modified MPS System. A modified version of our benchtop MPS system[11] added with a capacitor bank and a current feedback path was utilized for the optimization study experiments. Figure 1 shows a schematic representation of the modified MPS system that can be broken down into five different components: (1) a PC with pre-installed LabVIEW software to enable the system control; (2) a data acquisition unit (DAQ, NI USB-6289) for both the generation of sinusoids for excitation fields and subsequently the real-time collection of pick-up coil signals and passive current feedback information; (3) power amplifiers to amplify the high- and low-frequency excitation signals; (4) a switchable capacitor bank constituting individual resonating capacitors for different frequencies; and (5) a coil arrangement constituting two excitation coils to generate single- and dual-frequency magnetic fields along with a balanced set of pick-up coils. An electrical readout is generated from pick-up coils based on the magnetization response of MNPs following Faraday's law of induction ($\varepsilon = -N\Delta\varphi/\Delta t$). The total time for the collection of MPS readings was about 3 s. A further rest duration of 3 min was kept between multiple readings to avoid any heating of the coils. Ice packs were also kept across the coils to maintain stable temperatures. Fast Fourier transform is then applied to the captured electrical readout to analyze the harmonic response in different excitation scenarios. The presence of a current feedback loop enabled us to sense and control the magnetic field amplitude precisely while varying the excitation

https://doi.org/10.1021/acs.jpcc.2c07534
J. Phys. Chem. C 2023, 127, 450−460

Table 1. Sample Design Utilizing Single- and Multicore Nanoparticles for the MPS Optimization Study

sample index	MNPs used	MNP weight amount/vial (mg)	MNP molar amount/vial (fmole)	biological matrix	antibody amount
I	SHS30	0.016	544	PBS	NA
II		0.016	544	biotinylated antibodies	170.9 fmole
III	SuperMag50	0.04	40	PBS	NA
IV		0.04	40	biotinylated antibodies	106.8 fmole

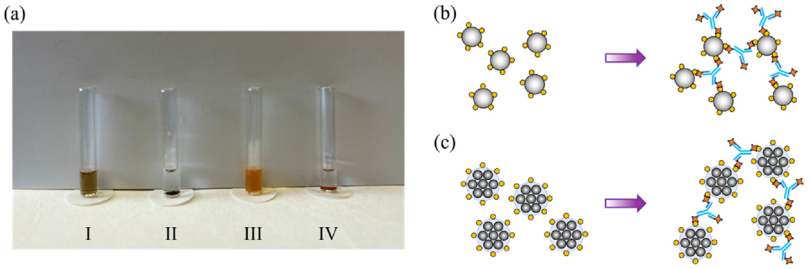

Figure 2. (a) Photograph of the prepared single-core SHS30 (vials I and II) and multicore SuperMag50 (vials III and IV) samples. Complete sedimentation of the MNPs was observed from vials II and IV in which excess amounts of biotinylated antibodies were added. Schematic presentation of the cluster formation of single-core and multicore MNPs presented, respectively, in (b) and (c).

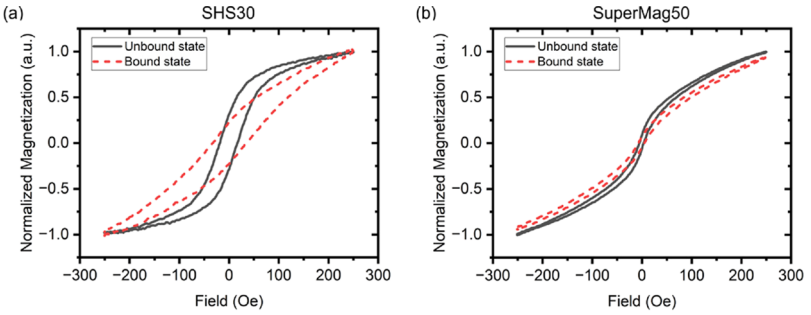

Figure 3. AC $M-H$ curves of (a) SHS30 and (b) SuperMag50 MNPs in the bound and unbound states.

field frequencies. Resonating capacitors allowed us to push the operational frequencies for both the high-frequency (f_H) and the low-frequency (f_L) excitation field signals to higher values while ensuring low reactive losses and thus maintaining a reasonably applied voltage level. More information on resonance effects and how these enable a high-frequency operation has been provided in the Supporting Information (Section S2).

2.4. Experimental Samples. Our experimental plans consisted of two sample groups utilizing SHS30 and SuperMag50 MNPs. Two samples were prepared for each group to simulate the unbound and bound states of the respective nanoparticles as listed in Table 1. It should be noted that although the weight concentrations of SHS30 and SuperMag50 MNPs are identical (1 mg/mL), the molar concentrations are different. Excess amounts of biotinylated antibodies were used to cause complete sedimentation of MNPs, as observed in Figure 2a. For the bound state samples, the SHS30 or SuperMag50 MNPs were mixed with biotinylated antibodies and incubated at 4 °C overnight. The consequent cluster formation due to streptavidin−biotin binding events for single- and multicore MNPs has been depicted in Figure 2b,c, respectively.

3. RESULTS AND DISCUSSIONS

3.1. Dynamic Magnetic Property Characterization of MNP Samples. The dynamic magnetization response of the MNP samples was studied under the application of a single-frequency AMF with an amplitude of 250 Oe and a frequency of 130 Hz. Dynamic property characterization was performed using the same modified benchtop scheme as described in Figure 1 with only the excitation of the low-frequency field coil. The magnetization response of the MNPs results in corresponding voltage generation in the balanced pick-up coil following Faraday's law of induction. This voltage response of the MNPs was then captured at a sampling rate of 100 ksps using the data acquisition channel of DAQ. The real-time voltage response along with the information on the applied magnetic field was then utilized to plot the dynamic magnetization−field ($M-H$) response curve following the methodology presented in the Supporting Information (Section S3). We do acknowledge that the magnetization response captured would look differently if captured under a different excitation frequency and/or magnetic field amplitude.[33]

Dynamic magnetization responses of both single-core SHS30 and multicore SuperMag50 MNPs in their bound and unbound states are presented in Figure 3a,b, respectively. In both plots, the response has been normalized to the highest magnetization values observed, namely, the unbound state of the respective MNPs. A clear difference in the AC $M-H$ loop can be observed from MNPs of the bound and unbound states in terms of increased coercivity and reduced remnant magnetization values. This change thus explains the reduction in the harmonic amplitude of the captured MPS spectra for

https://doi.org/10.1021/acs.jpcc.2c07534
J. Phys. Chem. C 2023, 127, 450−460

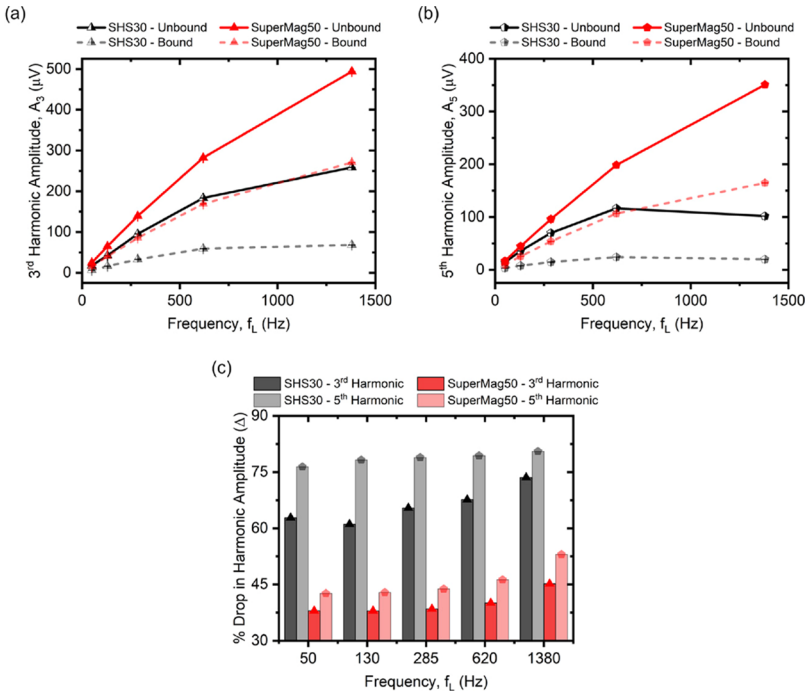

Figure 4. Frequency optimization results for the single-frequency system. (a,b) 3rd and 5th harmonic amplitudes recorded from SHS30 and SuperMag50 MNPs of the bound and unbound states. (c) Calculated % drop in the harmonic signal for both types of MNPs.

bound state nanoparticles as compared to the respective unbound state nanoparticles.

With this initial characterization of MNP samples done, further experiments were carried out to study the dependence of MPS spectra performance on the excitation field frequencies and amplitudes. The systematic experiments carried out for both single- and dual-frequency MPS systems for frequency and field amplitude optimizations have been presented with detailed analysis in Sections 3.2 and 3.3, respectively.

3.2. Frequency Optimization. Frequency optimization experiments were performed to study the dependence of harmonic spectra of MNPs on the excitation field frequencies in an MPS system. Experiments were designed to include frequency variations for both single- and dual-frequency MPS methodologies. For studying a single-frequency MPS modality, the voltage was applied only to the low-frequency coils from the system described in Figure 1 keeping the coil arrangements the same between experiments. However, for the dual-frequency experiments, both the low- and high-frequency coils were applied with a sinusoidal excitation signal. We will investigate the frequency optimization results for single- and dual-frequency systems in Sections 3.2.1 and 3.2.2, respectively.

3.2.1. Single-Frequency System. For the frequency optimization studies on the single-frequency system, MPS harmonic spectra were recorded with excitation of the low-frequency (f_L) coil at various frequency values while maintaining a constant field amplitude of 250 Oe. F_L was varied between 50 Hz, 130 Hz, 285 Hz, 620 Hz, and 1.38 kHz. The choice of these peculiar frequency numbers was due to the limited availability of unique capacitance values for the resonant capacitors. For each excitation frequency, we recorded the MPS spectrum and analyzed the changes in the 3rd and 5th harmonics observed at $3f_L$ and $5f_L$, respectively, for the single-excitation system. Figure 4a shows the frequency dependence of the 3rd harmonic response of the bound and unbound states for SHS30 and SuperMag50 MNPs. The results corresponding to the 5th harmonic variations are depicted in Figure 4b. We also calculated the % drop in the harmonic signal for the two states (defined as $\%\text{Drop}\ (\Delta) = \frac{A_{\text{Unbound State}} - A_{\text{Bound State}}}{A_{\text{Unbound State}}} \times 100$, where A stands for the harmonic amplitude), and the results have been presented in Figure 4c. From these readings, several key observations can be made. First, both the 3rd and the 5th harmonic amplitudes increase with an increment of the excitation frequency f_L for SHS30 as well as SuperMag50 MNPs. Second, Δ increases linearly for the single-core SHS30 MNPs and almost exponentially for the multicore SuperMag50 MNPs for the frequency range tested. Third, Δ is higher for the SHS30 MNPs as compared with the SuperMag50 in the observed frequency values. Δ can also be understood as the contribution of the Brownian relaxation mechanism to the harmonic response of an MNP, as Δ is the reduction in signal from a state allowing both Néel and Brownian relaxation simultaneously to a state allowing only Néel relaxation. This definition of Δ would be helpful in our further discussions. It should also be noted that the observations made above are valid for the frequency range mentioned previously.

3.2.2. Multiplexed Frequency System. For the multiplexed (dual-) frequency investigations, both low-frequency (f_L) and high-frequency (f_H) excitation fields were applied to MNPs. For this portion of the study, the goal was to examine the effect of the f_H variation while keeping all other parameters constant to limit the scope. Thus, to achieve this objective, the following experimental design was followed: (a) a low-frequency excitation signal was maintained at a constant operational frequency of f_L = 50 Hz and a constant field amplitude of 250 Oe; (b) the amplitude of the high-frequency field was maintained at 25 Oe while varying the excitation frequency f_H between 1 and 27 kHz. With this experimental design maintained, the 3rd and 5th harmonic responses (observed at f_H

https://doi.org/10.1021/acs.jpcc.2c07534
J. Phys. Chem. C 2023, 127, 450−460

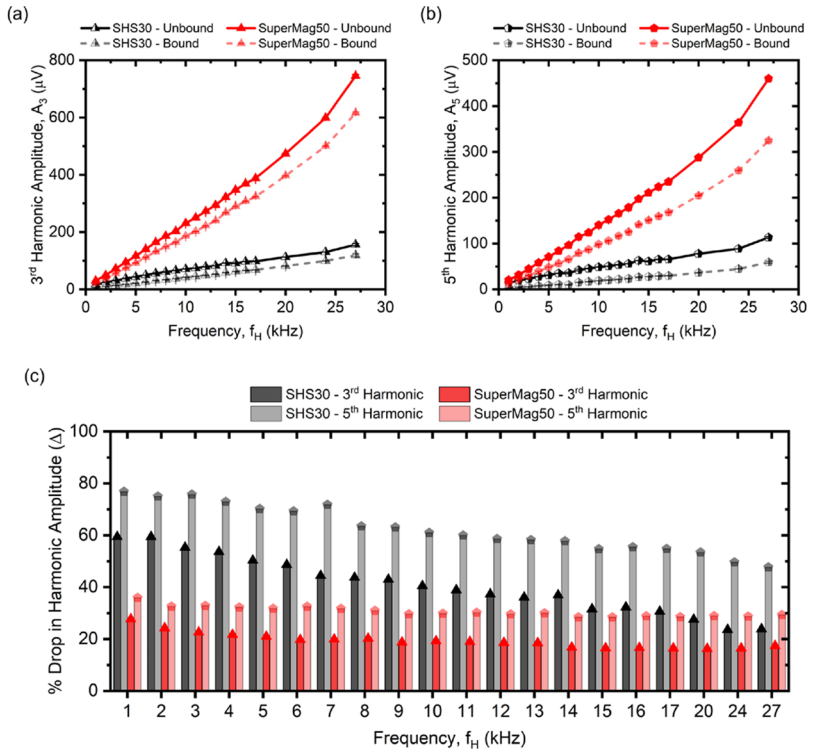

Figure 5. Frequency optimization results for the dual-frequency system. (a,b) 3rd and 5th harmonic amplitudes recorded from SHS30 and SuperMag50 MNPs of the bound and unbound states. (c) Calculated % drop in the harmonic signal for both types of MNPs.

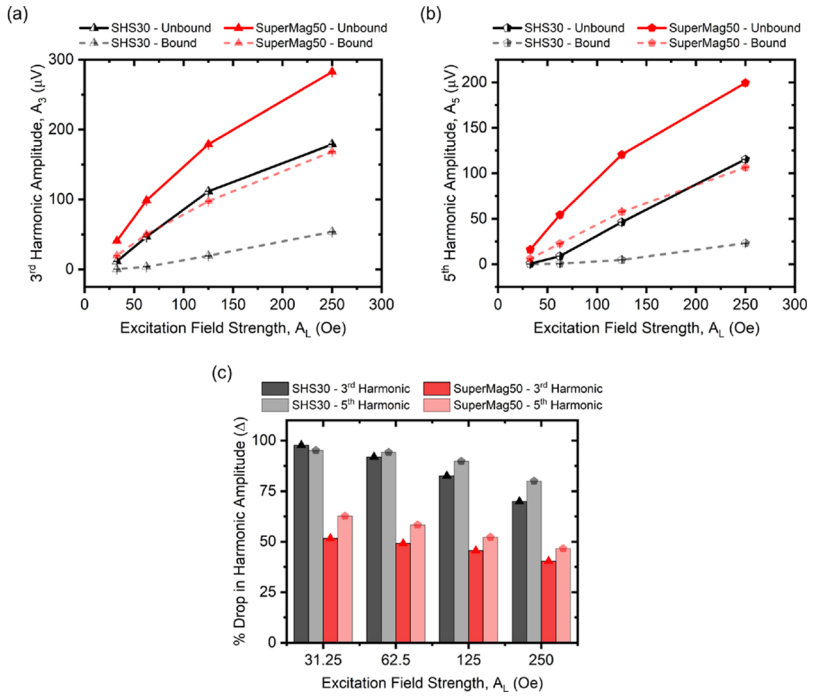

Figure 6. Amplitude optimization results for the single-frequency system. (a,b) 3rd and 5th harmonic amplitudes recorded from SHS30 and SuperMag50 MNPs of the bound and unbound states. (c) Calculated % drop in the harmonic signal for both types of MNPs.

+ $2f_L$ and $f_H + 4f_L$, respectively) of the bound and unbound MNP samples were recorded for the varying f_H values. The observed frequency dependence of the 3rd and the 5th harmonic amplitudes of MNPs has been summarized in Figure 5a,b. The signal drop in the respective harmonic amplitude, Δ, has also been presented in Figure 5c. Key takeaways from these observations were as follows: first, from all the samples, both the 3rd and the 5th harmonic amplitudes increase with the increase of f_H. Second, Δ decreases linearly for both the 3rd and the 5th harmonics of single-core SHS30 MNPs with an increment in the excitation frequency, f_H. Third, Δ drops consistently for the multicore SuperMag50 MNPs reaching a baseline saturation level around f_H = 14 kHz. Finally, the observed drop was persistently larger for harmonics of SHS30

https://doi.org/10.1021/acs.jpcc.2c07534
J. Phys. Chem. C 2023, 127, 450−460

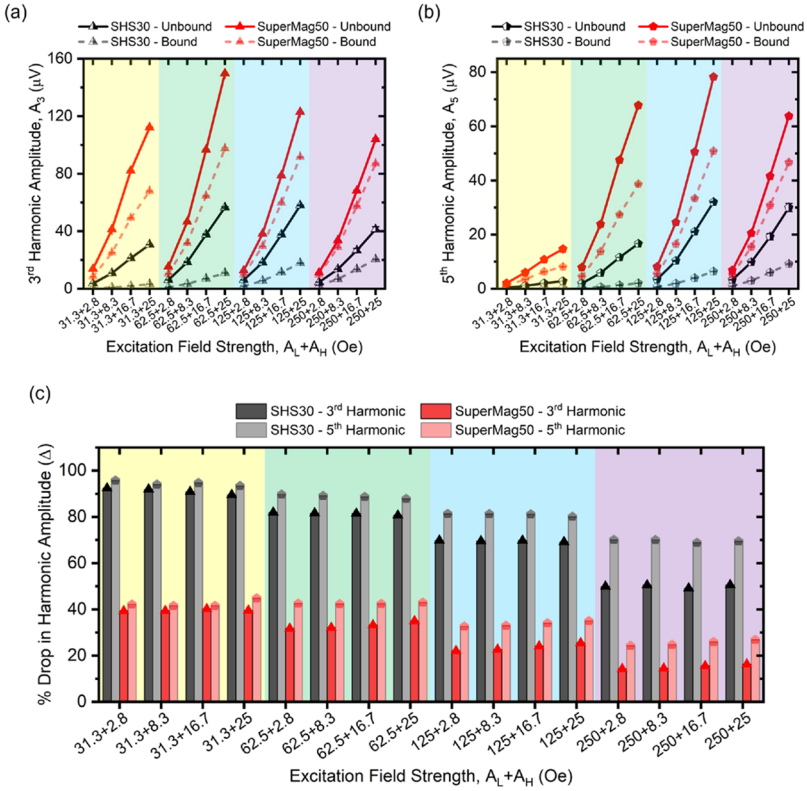

Figure 7. Amplitude optimization results for the dual-frequency system. (a,b) 3rd and 5th harmonic amplitudes recorded from SHS30 and SuperMag50 MNPs of the bound and unbound states. (c) Calculated % drop in the harmonic signal for both types of MNPs.

MNPs when compared to the drop in the respective harmonics of SuperMag50 MNPs for the frequency range in observation. We will once again use these observations in further sections to conclude the optimal operating conditions for bioassay applications.

3.3. Amplitude Optimization. Amplitude optimization studies were performed on the MNP samples by keeping the excitation frequencies, i.e., f_L and f_H constant while changing only the applied field amplitude. For a single-frequency MPS system, only the f_L excitation field was applied, and its amplitude A_L was varied. For a dual-frequency MPS setup, both f_L and f_H fields were applied, and their amplitudes, i.e., A_L and A_H were swept. A detailed study setup and results have been presented in the subsections.

3.3.1. Single-Frequency System. The amplitude optimization study for a single-frequency setup was carried out by keeping the field frequency f_L constant at 620 Hz and varying its amplitude A_L between 31.25, 62.5, 125, and 250 Oe. MPS spectra were recorded from all four samples, using each of the prior mentioned excitation conditions. Hence, in doing so, the dependence of both the 3rd and the 5th harmonic amplitudes on the excitation field amplitude was studied. Amplitudes of the 3rd and the 5th harmonics under varying excitation fields were summarized in Figure 6a,b, respectively. Similar to the frequency optimization studies, the drop in the respective harmonic amplitude was also calculated and has been plotted in Figure 6c. The key observations from this part of the study are as stated. First, the 3rd and the 5th harmonic amplitudes increase steadily for both bound and unbound states of the two types of MNPs with an increment in the applied field amplitude. Second, the drop in the harmonic amplitude from bound to unbound states, Δ, increases almost linearly with a decrement in A_L. Third, Δ for the 5th harmonic is decidedly larger than that of the 3rd harmonic. One abnormal reading of SHS30 MNPs for A_L = 31.25 Oe can be explained by the presence of small amplitudes of the harmonic magnitude for this case and the corresponding instrumentation recording error causing this issue. Fourth, Δ for SHS30 is observed to be larger than that for the SuperMag50 nanoparticles. These amplitude dependence results are in accordance with the theoretical models[34] for excitation field amplitude dependencies.

3.3.2. Multiplexed Frequency System. The following experimental design was followed for amplitude optimization studies using a multiplexed (dual-) frequency system: (1) field excitation frequencies f_L and f_H were kept constant at 50 Hz and 5 kHz, respectively. (2) The amplitude of the low-frequency field A_L was varied between 31.25, 62.5, 125, and 250 Oe. (3) For each magnitude of the low frequency applied, the high-frequency field amplitude A_H was varied between 2.78, 8.33, 16.67, and 25 Oe, and the MPS spectra were collected for all of the resulting 16 unique excitation scenarios. The 3rd and the 5th harmonic amplitude results from this part of the study have been presented in Figure 7a,b. The resultant harmonic drop (Δ) from the unbound state of MNPs to the maximum binding state has also been depicted in Figure 7c.

From these results obtained, the following insights can be drawn on the effect of the excitation field magnitude on the MNP harmonic spectra: (1) reducing the A_H amplitude leads to a monotonic reduction in both the 3rd and the 5th harmonic amplitudes for both the bound and the unbound MNP samples. (2) Reducing the A_L does not lead to a monotonic reduction in the respective harmonic amplitudes. The particular combinations producing the highest harmonic signal

https://doi.org/10.1021/acs.jpcc.2c07534
J. Phys. Chem. C 2023, 127, 450−460

for SHS30 and SuperMag50 MNPs in different states have been provided in Table 2. These findings indicate that the

Table 2. Combinations of Low- and High-Frequency Excitation Field Amplitudes, A_L and A_H, Generating the Highest Harmonic Amplitude for SHS30 and SuperMag50 MNPs

MNPs	rotational state	harmonic	A_L (Oe)	A_H (Oe)
SHS30	unbound state	3rd harmonic	125	25
		5th harmonic	125	25
	bound state	3rd harmonic	250	25
		5th harmonic	250	25
SuperMag50	unbound state	3rd harmonic	62.5	25
		5th harmonic	125	25
	bound state	3rd harmonic	62.5	25
		5th harmonic	125	25

choice of an excitation field for getting the highest harmonic amplitude is a function of all three factors, namely, (1) the choice of the nanoparticles, (2) the choice of the MPS harmonic, and (3) the conjugation state (bound or unbound) of MNPs for a particular application, i.e., for surface-based bioassay applications, one might want to maximize the harmonic amplitude from the bound state of nanoparticles, whereas for the volumetric bioassay applications, one might want to go with an excitation field magnitude choice, maximizing the harmonic amplitude from the unbound state and generating the highest Δ.

Similarly, the following observations regarding the drop in the harmonic amplitude can also be made: (1) reducing the A_H does not have a significant impact on Δ for either of the harmonics for both SHS30 and SuperMag50 nanoparticles; this can be observed from the relatively constant value of Δ for both the nanoparticles in Figure 7c when A_L is kept constant. (2) A significant increment in Δ is observed for both the 3rd and 5th harmonics of SHS30 and SuperMag50 nanoparticles with a reduction in the excitation field amplitude A_L. (3) Δ for single-core SHS30 nanoparticles is always greater than that observed for multicore SuperMag50 nanoparticles. (4) Finally, a drop in the 5th harmonic in all scenarios for both the nanoparticles is found to be larger as compared to the respective drop in the 3rd harmonic. We will look into the particular implications of these results on the bioassay methodologies in the following sections.

3.4. Volumetric Bioassays. With all the frequency and amplitude dependencies as studied above for the single-core SHS30 and the multicore SuperMag50 MNPs in both bound and unbound states, the key question of interest becomes what the optimum condition would be for the design of a bioassay system utilizing MPS or MPS-like methodologies. We try to answer this key question in this and the following section. In this section, we will discuss the implications for the design of a volumetric bioassay system, and in Section 3.5, we will investigate the operational design implications for surface-based bioassay systems.

The schematic view of a volumetric bioassay methodology for a dual-frequency MPS system has been depicted in Figure 8. Free MNPs in volumetric media can undergo both the Néel and Brownian relaxation processes simultaneously[35,36] and hence have a larger harmonic response in MPS spectra. However, upon the addition of target analytes, the MNPs undergo clustering events, thus restricting Brownian relaxation, which leads to a drop in the harmonic amplitude. Two important factors help improve the sensitivity of a volumetric bioassay MPS system: (1) Brownian dominant behavior of MNPs, what it means to our context is that a larger % drop (Δ) from the unbound state (simultaneous Brownian and Néel relaxation possible) to the bound state (only Néel relaxation possible) benefits sensitivity; and (2) higher harmonic amplitude from unbound MNPs, this has an indirect effect on sensitivity as it allows for the use of smaller quantities of MNPs for bioassay testing, which has proven to improve the sensitivity significantly.[37,38] Because of this unique dependence, instead of giving general guidelines, we will limit ourselves to only a few categorical reviews that can help improve sensitivity.

For a single-frequency MPS system, increasing the excitation frequency f_L positively improves both the harmonic amplitude from unbound MNPs and corresponding Δ, so the use of higher excitation frequencies can help with sensitivity improvement. Also, for the single-frequency MPS system, increasing the excitation field amplitude increases the harmonic amplitude significantly but also leads to a small reduction in Δ. Due to the relative scale of changes as observed from Figure 6, i.e., greater than 10 times improvement in the harmonic amplitude, and only around 25% reduction in corresponding Δ for the A_L variation, an argument can be made that a larger excitation field is also beneficial for the overall sensitivity.

For a dual-frequency system, the excitation field amplitude combination (A_L + A_H) of 62.5 Oe + 25 Oe results in a higher harmonic amplitude together with a significant improvement in Δ when compared to the excitation scenario of 250 Oe + 25 Oe excitation fields. This implies that a larger excitation signal is not necessarily the most optimal for bioassay applications. In the excitation frequency case, the scenario is much more complex as increasing the f_H increases the harmonic amplitude significantly but also leads to a significant reduction in Δ (refer to Figure 5). Hence, a coherent sensitivity argument cannot be

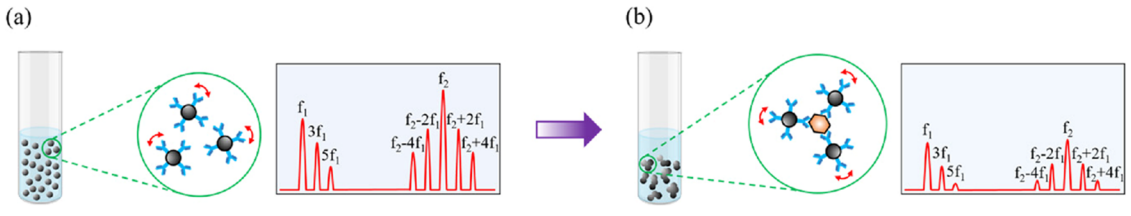

Figure 8. Schematic depiction of the harmonic change in a volumetric bioassay process for a dual-excitation field MPS system. (a) MNPs coated with polyclonal capture antibodies are free to rotate in the test volume. (b) Addition of the biological sample constituting a target analyte causes cluster formation and increases the hydrodynamic size. This increment in the hydrodynamic size leads to a higher phase lag in the Brownian relaxation process, causing a reduction in the harmonic amplitude.

https://doi.org/10.1021/acs.jpcc.2c07534
J. Phys. Chem. C 2023, 127, 450−460

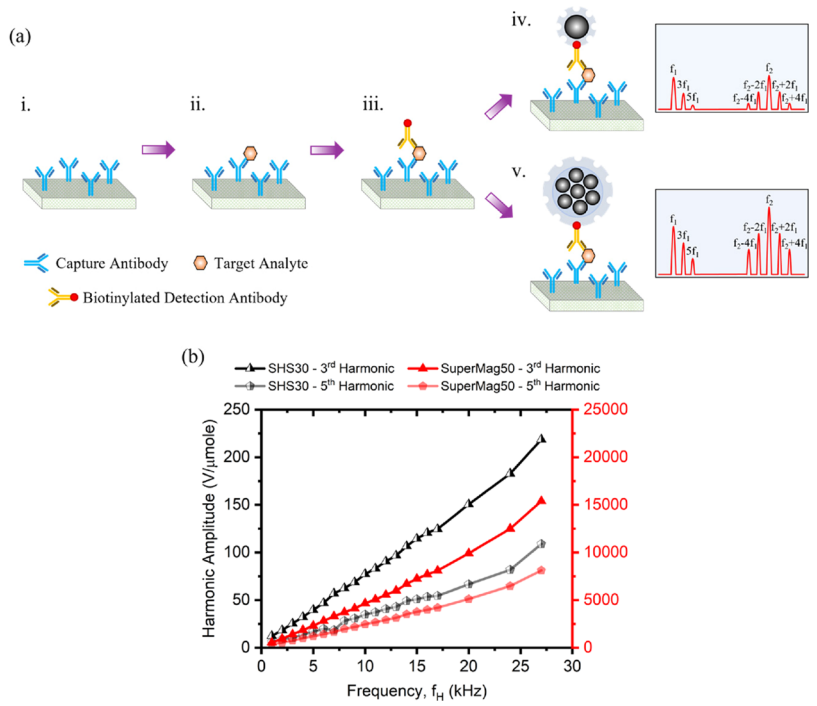

Figure 9. (a) Schematic representation of a surface-conjugation-based MPS bioassay mechanism along with the harmonic signal generation for single- and multicore nanoparticles. (i) Capture antibodies are immobilized on a reaction surface. (ii) In addition to the biological test sample constituting a target analyte, the target analyte specifically binds to the capture antibodies. (iii) Biotinylated detection antibodies are immobilized on the target analyte completing the sandwich assay structure. Streptavidin-coated nanoparticles are then captured on the biotinylated detection antibodies; this process for single- and multicore MNPs has been shown in (iv) and (v), respectively, with corresponding resultant MPS harmonic spectra. (b) Harmonic amplitude per micro-mole of the bound state of MNPs for SHS30 and SuperMag50 has been depicted.

made without conducting further tests to determine the limit of detection for each case.

3.5. Surface-Based Bioassays. In surface-based bioassay methodologies, the MNPs are immobilized on a reaction surface following the sandwich bioassay mechanism. A schematic view of a sandwich bioassay scheme is depicted in Figure 9a along with the resultant harmonic spectra from immobilized MNPs. Immobilized MNPs can only undergo the Néel relaxation process once an excitation field is applied. This is also the case for the bound state of MNPs where complete sedimentation of nanoparticles can be observed (refer to Figure 2), i.e., samples II and IV, pertaining to strong streptavidin−biotin binding and excess amounts of biotinylated antibodies added. Hence, by looking specifically at the harmonic amplitudes of the bound state SHS30 and SuperMag50 nanoparticles, intuitive arguments can be made regarding the choice of nanoparticles and the MPS excitation methodology for optimum bioassay performance. It should also be pointed out here that this study was limited to the use of single-core SHS30 and multicore SuperMag50 nanoparticles, and a choice of a different set of MNPs can result in uniquely different observations.

First, for the choice between a single- and a dual-frequency MPS methodology, the latter is more favorable. This can be argued by the observation that although increasing the excitation frequency in either of the methodologies leads to a monotonous increment in the harmonic amplitudes, in the case of single-frequency excitation, it also leads to a significant increment in Δ, which is not the case observed for the dual-frequency excitation scenarios. Second, the use of multicore SuperMag50 MNPs is several orders better than the use of single-core SHS30 MNPs. The argument for this peculiar choice of MNPs can be understood from the findings presented in Figure 9b, which shows the results for the harmonic amplitude generated per micro-mole of the bound state of MNPs for both sets of nanoparticles. It can be noted that SuperMag50 generates a significantly larger harmonic response per micro-mole of nanoparticles. This can be attributed to two main reasons: (1) SuperMag50 MNPs show a strong Néel dominant relaxation mechanism for dual-excitation MPS systems, as can be inferred from Figure 5b. (2) SuperMag50 MNPs are made of a cluster of smaller nanoparticles fixed in a matrix and hence have a high magnetic moment generated per particle as compared to SHS30. Finally, the use of a higher excitation frequency f_H is favorable for the surface-based MPS bioassay systems.

4. CONCLUSIONS AND FUTURE PROSPECTS

Herein, we study the effects of the excitation field amplitude and frequency modulation on the MPS spectra of single-core SHS30 and multicore SuperMag50 MNPs. The modulation study was performed for both the single- and dual-frequency MPS schemes to uniquely identify the optimization conditions that can improve the bioassay system sensitivities. For these experiments, MNP samples in unbound and bound states were prepared to simulate (1) border scenarios of a volumetric bioassay scheme and (2) immobilization scenarios of a surface-based bioassay scheme. Streptavidin-coated nanoparticles were added with excess amounts of biotinylated antibodies to cause aggregation and complete sedimentation to realize the bound state. To identify the optimal scenarios for surface-based bioassay applications, the harmonic signal from the bound state of nanoparticles was chosen to be the determining factor; to note the favorable conditions for volumetric bioassay

https://doi.org/10.1021/acs.jpcc.2c07534
J. Phys. Chem. C 2023, 127, 450−460

systems, a higher harmonic signal from an unbound state of MNPs together with higher Δ were chosen to be the deciding factors for optimized performance. Although the use of Faraday detection coils would suggest that the choice of a higher excitation frequency and a high excitation field amplitude should favor a larger harmonic response from nanoparticles, the observations show that an upper limit is imposed by the MNP's relaxation time instead. The key findings were noted as described below.

The experimental results demonstrate the distinct advantages of choosing multicore MNPs for use with dual-excitation frequency MPS systems in surface-based bioassays. We further noted that for this modality, modulating the excitation field frequency and amplitude could further improve the system sensitivities. First, for the optimal frequency selection, a higher excitation frequency was found to be favorable as it generated a higher harmonic signal from the same MNP amount. Second, for the optimal excitation field amplitude selection, it was found that for SuperMag50 multicore MNPs, an A_L = 62.5 Oe and A_H = 25 Oe combination resulted in the highest harmonic signal from the bound state of nanoparticles.

For the volumetric bioassays, both single- and multicore MNPs in conjunction with the use of a single-excitation frequency MPS system were found to be suitable candidates. As can be noted from Figures 4 and 5, the single-frequency systems resulted in a significantly higher Δ while providing better (in the case of single-core MNPs) or equivalent (in the case of multicore MNPs) harmonic spectra amplitudes from the unbound state of nanoparticles when compared to the dual-excitation MPS systems. Furthermore, it was found that for the single-excitation frequency MPS scheme, the use of both a higher excitation frequency f_L and a larger excitation field strength A_L provides significant improvements in the MNP harmonic spectra amplitude and the resultant harmonic drop (Δ). Both favor the scenarios for sensitivity improvement in the case of volumetric bioassays. In this study, however, we do not comment on the choice of single- or multicore MNPs being the better candidate for the volumetric bioassay application. On one hand, single-core MNPs present with a larger harmonic drop, meaning that the Brownian relaxation mechanism is more dominant for these nanoparticles; on the other hand, they also offer a smaller harmonic amplitude. This means that a smaller number of multicore MNPs can be utilized instead for the generation of a suitable harmonic amplitude for bioassay applications, which has been shown to provide significant sensitivity improvements.[37,38] Due to this dichotomy between the harmonic amplitude strength and corresponding Δ, the choice between single- or multicore MNPs for better sensitivity has been left for further in-depth investigation.

■ ASSOCIATED CONTENT

Supporting Information

The Supporting Information is available free of charge at https://pubs.acs.org/doi/10.1021/acs.jpcc.2c07534.

Static magnetization response curves for SHS30 and SuperMag50 MNPs; SPICE modeling of the resonance effects to enable high-frequency, high-magnetic-field operation; and dynamic magnetic property characterization using a single-frequency MPS system (PDF)

■ AUTHOR INFORMATION

Corresponding Authors

Kai Wu − *Department of Electrical and Computer Engineering, University of Minnesota, Minneapolis, Minnesota 55455, United States;* Present Address: Department of Electrical and Computer Engineering, Texas Tech University, Lubbock, Texas 79409, United States (K.W.); orcid.org/0000-0002-9444-6112; Email: kai.wu@ttu.edu

Maxim C-J Cheeran − *Department of Veterinary Population Medicine, University of Minnesota, St. Paul, Minnesota 55108, United States*; Email: cheeran@umn.edu

Jian-Ping Wang − *Department of Electrical and Computer Engineering, University of Minnesota, Minneapolis, Minnesota 55455, United States;* orcid.org/0000-0002-0687-3203; Email: jpwang@umn.edu

Authors

Vinit Kumar Chugh − *Department of Electrical and Computer Engineering, University of Minnesota, Minneapolis, Minnesota 55455, United States;* orcid.org/0000-0001-7818-7811

Arturo di Girolamo − *Department of Electrical and Computer Engineering, University of Minnesota, Minneapolis, Minnesota 55455, United States*

Venkatramana D. Krishna − *Department of Veterinary Population Medicine, University of Minnesota, St. Paul, Minnesota 55108, United States;* orcid.org/0000-0002-1980-5525

Complete contact information is available at: https://pubs.acs.org/10.1021/acs.jpcc.2c07534

Notes

The authors declare no competing financial interest.

■ ACKNOWLEDGMENTS

This study was financially supported by the Institute of Engineering in Medicine, the Robert F. Hartmann Endowed Chair professorship, the University of Minnesota Medical School, and the University of Minnesota Physicians and Fairview Health Services through a COVID-19 Rapid Response Grant. This study was also financially supported by the U.S. Department of Agriculture − National Institute of Food and Agriculture (NIFA) under the Award Number 2020-67021-31956. Research reported in this publication was supported by the National Institute of Dental and Craniofacial Research of the National Institutes of Health under the Award Number R42DE030832. The content is solely the responsibility of the authors and does not necessarily represent the official views of the National Institutes of Health. Portions of this study were conducted in the Minnesota Nano Center, which is supported by the National Science Foundation through the National Nano Coordinated Infrastructure Network (NNCI) under the Award Number ECCS-1542202.

■ REFERENCES

(1) Gleich, B.; Weizenecker, J. Tomographic Imaging Using the Nonlinear Response of Magnetic Particles. *Nature* **2005**, *435*, 1214−1217.

(2) Panagiotopoulos, N.; Duschka, R. L.; Ahlborg, M.; Bringout, G.; Debbeler, C.; Graeser, M.; Kaethner, C.; Lüdtke-Buzug, K.; Medimagh, H.; Stelzner, J.; et al. Magnetic Particle Imaging: Current

Developments and Future Directions. *Int. J. Nanomed.* **2015**, *10*, 3097−3114.
(3) Krause, H.-J.; Wolters, N.; Zhang, Y.; Offenhäusser, A.; Miethe, P.; Meyer, M. H. F.; Hartmann, M.; Keusgen, M. Magnetic Particle Detection by Frequency Mixing for Immunoassay Applications. *J. Magn. Magn. Mater.* **2007**, *311*, 436−444.
(4) Nikitin, P. I.; Vetoshko, P. M.; Ksenevich, T. I. New Type of Biosensor Based on Magnetic Nanoparticle Detection. *J. Magn. Magn. Mater.* **2007**, *311*, 445−449.
(5) Khurshid, H.; Friedman, B.; Berwin, B.; Shi, Y.; Ness, D. B.; Weaver, J. B. Blood Clot Detection Using Magnetic Nanoparticles. *AIP Adv.* **2017**, *7*, No. 056723.
(6) Wu, K.; Liu, J.; Wang, Y.; Ye, C.; Feng, Y.; Wang, J.-P. Superparamagnetic Nanoparticle-Based Viscosity Test. *Appl. Phys. Lett.* **2015**, *107*, No. 053701.
(7) Orlov, A. V.; Khodakova, J. A.; Nikitin, M. P.; Shepelyakovskaya, A. O.; Brovko, F. A.; Laman, A. G.; Grishin, E. V.; Nikitin, P. I. Magnetic Immunoassay for Detection of Staphylococcal Toxins in Complex Media. *Anal. Chem.* **2013**, *85*, 1154−1163.
(8) Orlov, A. V.; Znoyko, S. L.; Cherkasov, V. R.; Nikitin, M. P.; Nikitin, P. I. Multiplex Biosensing Based on Highly Sensitive Magnetic Nanolabel Quantification: Rapid Detection of Botulinum Neurotoxins A, B, and E in Liquids. *Anal. Chem.* **2016**, *88*, 10419−10426.
(9) Achtsnicht, S.; Neuendorf, C.; Faßbender, T.; Nölke, G.; Offenhäusser, A.; Krause, H.-J.; Schröper, F. Sensitive and Rapid Detection of Cholera Toxin Subunit B Using Magnetic Frequency Mixing Detection. *PLoS One* **2019**, *14*, No. e0219356.
(10) Pietschmann, J.; Spiegel, H.; Krause, H.-J.; Schillberg, S.; Schröper, F. Sensitive Aflatoxin B1 Detection Using Nanoparticle-Based Competitive Magnetic Immunodetection. *Toxins* **2020**, *12*, 337.
(11) Wu, K.; Liu, J.; Saha, R.; Su, D.; Krishna, V. D.; Cheeran, M. C.-J.; Wang, J.-P. Magnetic Particle Spectroscopy for Detection of Influenza A Virus Subtype H1N1. *ACS Appl. Mater. Interfaces* **2020**, *12*, 13686−13697.
(12) Zhong, J.; Rösch, E. L.; Viereck, T.; Schilling, M.; Ludwig, F. Toward Rapid and Sensitive Detection of SARS-CoV-2 with Functionalized Magnetic Nanoparticles. *ACS Sens.* **2021**, *6*, 976−984.
(13) Pietschmann, J.; Voepel, N.; Voß, L.; Rasche, S.; Schubert, M.; Kleines, M.; Krause, H.-J.; Shaw, T. M.; Spiegel, H.; Schroeper, F. Development of Fast and Portable Frequency Magnetic Mixing-Based Serological SARS-CoV-2-Specific Antibody Detection Assay. *Front. Microbiol.* **2021**, *12*, No. 643275.
(14) Wu, K.; Chugh, V. K.; Krishna, V. D.; di Girolamo, A.; Wang, Y. A.; Saha, R.; Liang, S.; Cheeran, M. C.-J.; Wang, J.-P. One-Step, Wash-Free, Nanoparticle Clustering-Based Magnetic Particle Spectroscopy Bioassay Method for Detection of SARS-CoV-2 Spike and Nucleocapsid Proteins in the Liquid Phase. *ACS Appl. Mater. Interfaces* **2021**, *13*, 44136−44146.
(15) Hong, H.-B.; Krause, H.-J.; Song, K.-B.; Choi, C.-J.; Chung, M.-A.; Son, S.; Offenhäusser, A. Detection of Two Different Influenza A Viruses Using a Nitrocellulose Membrane and a Magnetic Biosensor. *J. Immunol. Methods* **2011**, *365*, 95−100.
(16) Bragina, V. A.; Orlov, A. V.; Znoyko, S. L.; Pushkarev, A. V.; Novichikhin, D. O.; Guteneva, N. V.; Nikitin, M. P.; Gorshkov, B. G.; Nikitin, P. I. Nanobiosensing Based on Optically Selected Antibodies and Superparamagnetic Labels for Rapid and Highly Sensitive Quantification of Polyvalent Hepatitis B Surface Antigen. *Anal. Methods* **2021**, *13*, 2424−2433.
(17) Rösch, E. L.; Zhong, J.; Lak, A.; Liu, Z.; Etzkorn, M.; Schilling, M.; Ludwig, F.; Viereck, T.; Lalkens, B. Point-of-Need Detection of Pathogen-Specific Nucleic Acid Targets Using Magnetic Particle Spectroscopy. *Biosens. Bioelectron.* **2021**, *192*, No. 113536.
(18) Rettcher, S.; Jungk, F.; Kühn, C.; Krause, H.-J.; Nölke, G.; Commandeur, U.; Fischer, R.; Schillberg, S.; Schröper, F. Simple and Portable Magnetic Immunoassay for Rapid Detection and Sensitive Quantification of Plant Viruses. *Appl. Environ. Microbiol.* **2015**, *81*, 3039−3048.
(19) Orlov, A. V.; Bragina, V. A.; Nikitin, M. P.; Nikitin, P. I. Rapid Dry-Reagent Immunomagnetic Biosensing Platform Based on Volumetric Detection of Nanoparticles on 3D Structures. *Biosens. Bioelectron.* **2016**, *79*, 423−429.
(20) Gordon-Wylie, S. W.; Ness, D. B.; Shi, Y.; Mirza, S. K.; Paulsen, K. D.; Weaver, J. B. Measuring Protein Biomarker Concentrations Using Antibody Tagged Magnetic Nanoparticles. *Biomed. Phys. Eng. Express* **2020**, *6*, No. 065025.
(21) Wu, K.; Su, D.; Saha, R.; Liu, J.; Chugh, V. K.; Wang, J.-P. Magnetic Particle Spectroscopy: A Short Review of Applications Using Magnetic Nanoparticles. *ACS Appl. Nano Mater.* **2020**, *3*, 4972−4989.
(22) Bragina, V. A.; Khomyakova, E.; Orlov, A. V.; Znoyko, S. L.; Mochalova, E. N.; Paniushkina, L.; Shender, V. O.; Erbes, T.; Evtushenko, E. G.; Bagrov, D. V.; et al. Highly Sensitive Nanomagnetic Quantification of Extracellular Vesicles by Immunochromatographic Strips: A Tool for Liquid Biopsy. *Nanomaterials* **2022**, *12*, 1579.
(23) Zhang, X.; Reeves, D. B.; Perreard, I. M.; Kett, W. C.; Griswold, K. E.; Gimi, B.; Weaver, J. B. Molecular Sensing with Magnetic Nanoparticles Using Magnetic Spectroscopy of Nanoparticle Brownian Motion. *Biosens. Bioelectron.* **2013**, *50*, 441−446.
(24) Khurshid, H.; Shi, Y.; Berwin, B. L.; Weaver, J. B. Evaluating Blood Clot Progression Using Magnetic Particle Spectroscopy. *Med. Phys.* **2018**, *45*, 3258−3263.
(25) Weaver, J. B.; Ness, D. B.; Fields, J.; Jyoti, D.; Gordon-Wylie, S. W.; Berwin, B. L.; Mirza, S.; Fiering, S. N. Identifying *in Vivo* Inflammation Using Magnetic Nanoparticle Spectra. *Phys. Med. Biol.* **2020**, *65*, 125003.
(26) Chieh, J. J.; Yang, S. Y.; Jian, Z. F.; Wang, W. C.; Horng, H. E.; Yang, H. C.; Hong, C.-Y. Hyper-High-Sensitivity Wash-Free Magnetoreduction Assay on Biomolecules Using High-Tc Superconducting Quantum Interference Devices. *J. Appl. Phys.* **2008**, *103*, No. 014703.
(27) Chiu, M. J.; Horng, H. E.; Chieh, J. J.; Liao, S. H.; Chen, C. H.; Shih, B. Y.; Yang, C. C.; Lee, C. L.; Chen, T. F.; Yang, S. Y.; et al. Multi-Channel SQUID-Based Ultra-High-Sensitivity In-Vitro Detections for Bio-Markers of Alzheimer's Disease Via Immunomagnetic Reduction. *IEEE Trans. Appl. Supercond.* **2011**, *21*, 477−480.
(28) Yang, S.-Y.; Liu, H.-C.; Chen, W.-P. Immunomagnetic Reduction Detects Plasma Aβ1−42 Levels as a Potential Dominant Indicator Predicting Cognitive Decline. *Neurol. Ther.* **2020**, *9*, 435−442.
(29) Meyer, M. H. F.; Krause, H.-J.; Hartmann, M.; Miethe, P.; Oster, J.; Keusgen, M. Francisella Tularensis Detection Using Magnetic Labels and a Magnetic Biosensor Based on Frequency Mixing. *J. Magn. Magn. Mater.* **2007**, *311*, 259−263.
(30) Guteneva, N. V.; Znoyko, S. L.; Orlov, A. V.; Nikitin, M. P.; Nikitin, P. I. Rapid Lateral Flow Assays Based on the Quantification of Magnetic Nanoparticle Labels for Multiplexed Immunodetection of Small Molecules: Application to the Determination of Drugs of Abuse. *Microchim. Acta* **2019**, *186*, 621.
(31) Kim, C.-B.; Lim, E.-G.; Shin, S. W.; Krause, H. J.; Hong, H. Magnetic Immunoassay Platform Based on the Planar Frequency Mixing Magnetic Technique. *Biosens. Bioelectron.* **2016**, *83*, 293−299.
(32) Znoyko, S. L.; Orlov, A. V.; Pushkarev, A. V.; Mochalova, E. N.; Guteneva, N. V.; Lunin, A. V.; Nikitin, M. P.; Nikitin, P. I. Ultrasensitive Quantitative Detection of Small Molecules with Rapid Lateral-Flow Assay Based on High-Affinity Bifunctional Ligand and Magnetic Nanolabels. *Anal. Chim. Acta* **2018**, *1034*, 161−167.
(33) Draack, S.; Lucht, N.; Remmer, H.; Martens, M.; Fischer, B.; Schilling, M.; Ludwig, F.; Viereck, T. Multiparametric Magnetic Particle Spectroscopy of $CoFe_2O_4$ Nanoparticles in Viscous Media. *J. Phys. Chem. C* **2019**, *123*, 6787−6801.
(34) Wu, K.; Tu, L.; Su, D.; Wang, J.-P. Magnetic Dynamics of Ferrofluids: Mathematical Models and Experimental Investigations. *J. Phys. D: Appl. Phys.* **2017**, *50*, No. 085005.
(35) Draack, S.; Viereck, T.; Nording, F.; Janssen, K.-J.; Schilling, M.; Ludwig, F. Determination of Dominating Relaxation Mechanisms

https://doi.org/10.1021/acs.jpcc.2c07534
J. Phys. Chem. C 2023, 127, 450−460

from Temperature-Dependent Magnetic Particle Spectroscopy Measurements. *J. Magn. Magn. Mater.* **2019**, *474*, 570−573.
(36) Wu, K.; Su, D.; Saha, R.; Wong, D.; Wang, J.-P. Magnetic Particle Spectroscopy-Based Bioassays: Methods, Applications, Advances, and Future Opportunities. *J. Phys. D: Appl. Phys.* **2019**, *52*, 173001.
(37) Zhong, J.; Janssen, K.-J.; Draack, S.; Viereck, T.; Schilling, M.; Ludwig, F. Dependence of Biomolecule Detection on Magnetic Nanoparticle Concentration. *J. Magn. Magn. Mater.* **2021**, *517*, No. 167408.
(38) Chugh, V. K.; Wu, K.; Krishna, V. D.; di Girolamo, A.; Bloom, R. P.; Wang, Y. A.; Saha, R.; Liang, S.; Cheeran, M. C.-J.; Wang, J.-P. Magnetic Particle Spectroscopy with One-Stage Lock-In Implementation for Magnetic Bioassays with Improved Sensitivities. *J. Phys. Chem. C* **2021**, *125*, 17221−17231.

https://doi.org/10.1021/acs.jpcc.2c07534
J. Phys. Chem. C 2023, 127, 450−460